Supplementary Information for

Multi-proteomics unveils host perturbations by tick-borne encephalitis virus for intervention targets

Liyan Sui, Wenfang Wang, Xuerui Guo, Yinghua Zhao, Tian Tian, Jinlong Zhang, Heming Wang, Yueshan Xu, Hongmiao Chi, Hanxi Xie, Wenbo Xu, Nan Liu, Li Zhao, Guangqi Song, Zhedong Wang, Kaiyu Zhang, Lihe Che, Yicheng Zhao*, Guoqing Wang*, Quan Liu*

* Correspondence: qing@jlu.edu.cn (G.W.); yichengzhao@live.cn (Y. Z.); liuquan1973@hotmail.com (Q. L.).

This PDF file includes:

Supplementary Figures S1 to S17

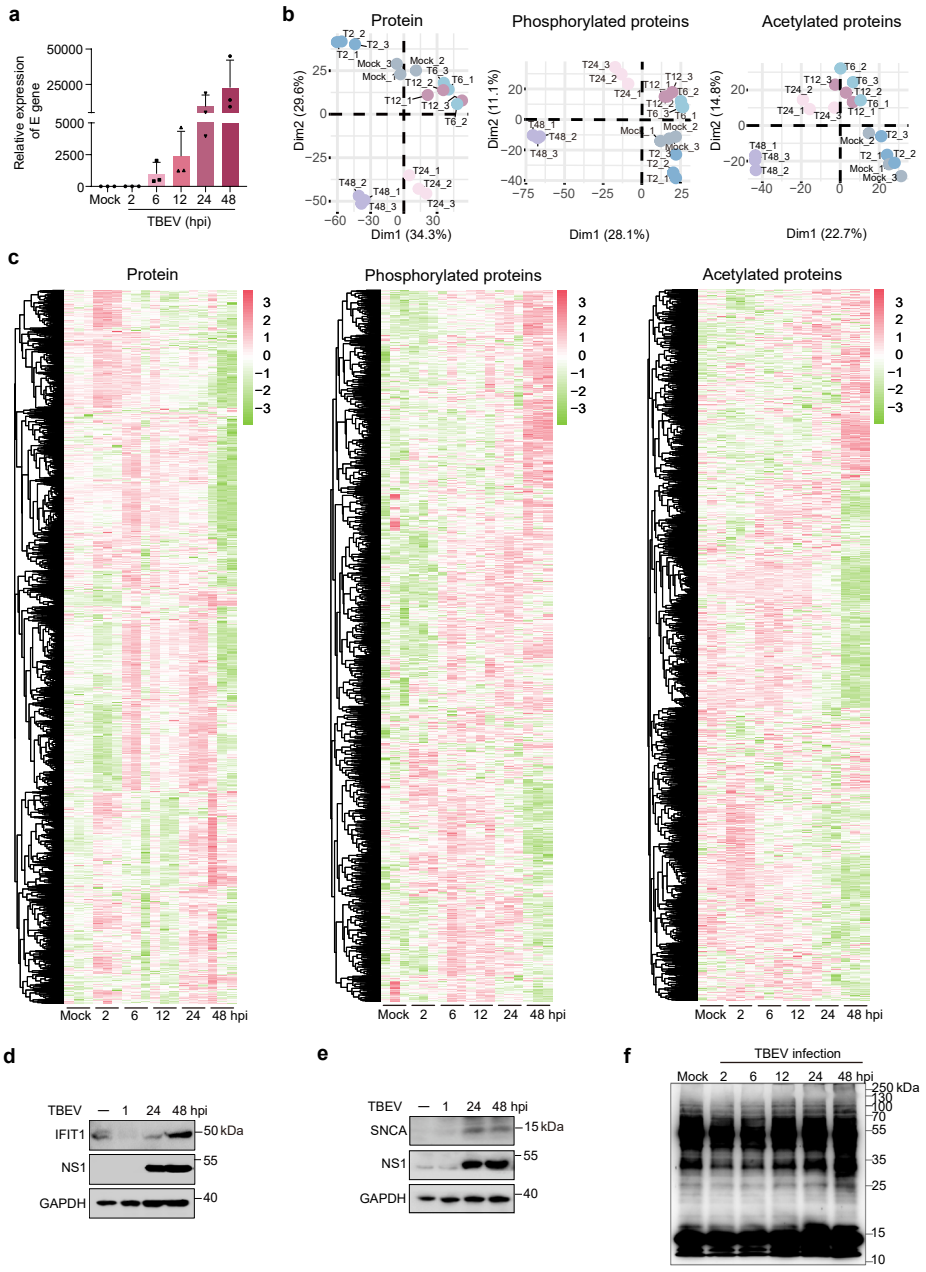

Figure S1. Quality control of multi-omics analysis of cells infected with TBEV

a. Gradual increase in the copies of TBEV E genes with the duration of TBEV infection, as quantified by probe PCR. Each point represents a sample. Data are represented as mean ± SEM of 3 independent experiments. The P-values are calculated and reported using one-way ANOVA. Source data are provided as a Source Data file.

b. Principal component analysis (PCA) plots depicting good separation of samples at different timepoints during TBEV infection, analyzed by proteomics (left), phosphoproteome (middle), and acetylproteome (right).

c. Heatmaps displaying the expression levels of proteins (left), phosphorylated proteins (middle) and acetylated proteins (right) across triplicate samples at each time point.

d, e. Immunoblot analysis demonstrating increased expression levels of IFIT1 and SNCA upon TBEV infection, based on data from three independent trials.

f. Positive correlation observed between the acetylation level of TBEV-infected cells and the duration of TBEV infection analyzed by immunoblotting with pan-Acetylation antibody, based on data from three independent trials.

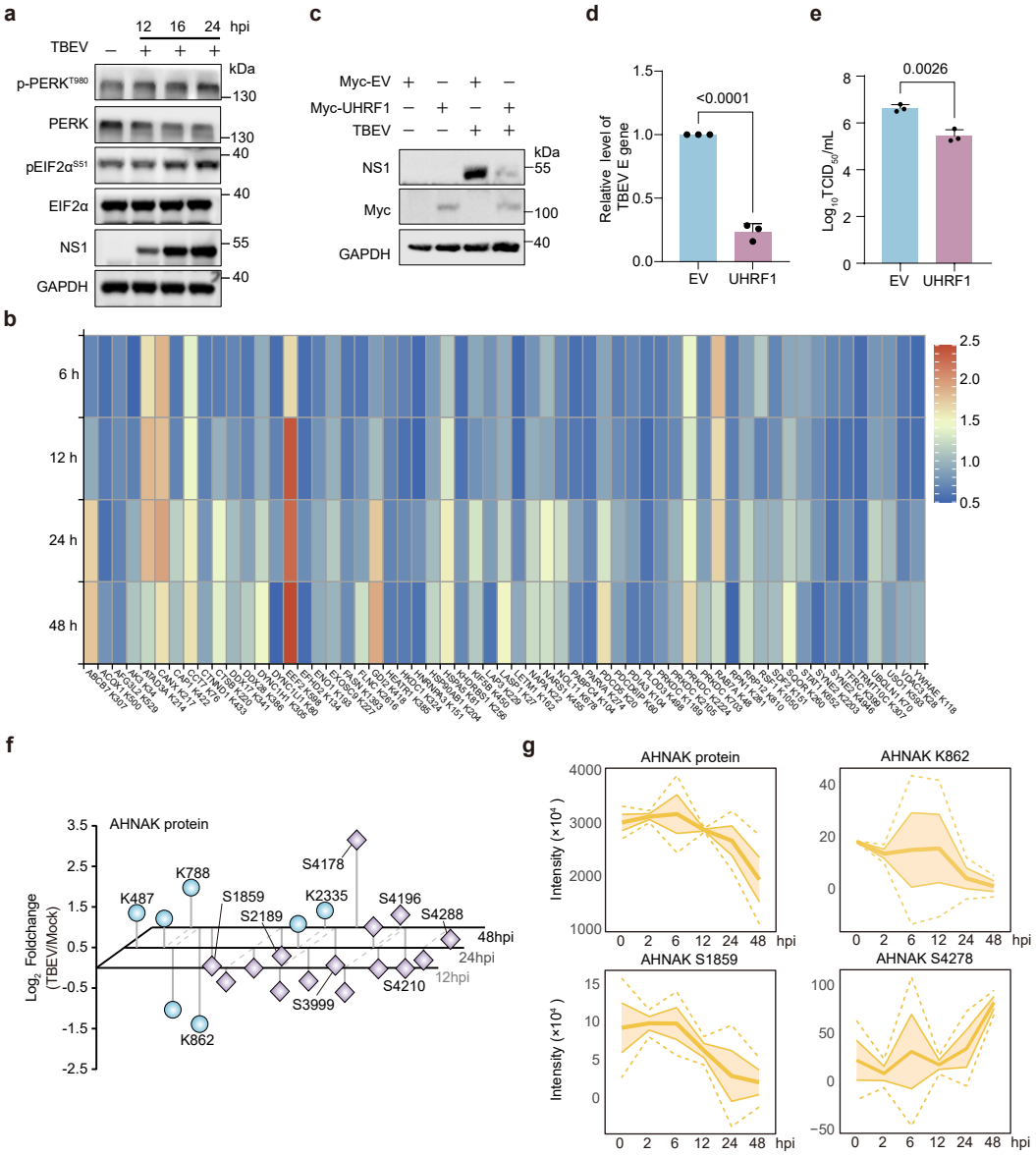

Figure S2. Acetylation and phosphorylation of host proteins during TBEV infection

a. Immunoblot assay showed an increase in the phosphorylated forms of PERK (T980) and EIF-2α (S51) in cells infected with TBEV at 12, 16 and 24 hpi, based on data from three independent trials.

b. Significant changed acetylation sites at both 6, 12, 24 and 48 h upon TBEV infection.

c-e. In cells transfected with Myc-UHRF1, TBEV NS1 protein (**c**), E genes (**d**) and viral titers (**e**) significantly decreased compared to cells transfected with Myc-EV (empty vector). Each point represents a sample. Data are represented as mean ± SEM of 3 independent experiments. The P-values are calculated and reported using one-way ANOVA. Source data are provided as a Source Data file.

f. Significantly regulated phosphorylation (purple squares) and acetylation (blue circles) sites on

AHANK during TBEV infection. The plot depicts median changes in the abundance of phosphorylation and acetylation sites compared with the mock infection group at 12, 24 and 48 hpi.

g. Regulation of protein abundance, K862 acetylation, S1859 and S4278 phosphorylation of AHANK in TBEV-infected cells. The median is represented by the line, the 50% range shown as the shaded region, and the 95% confidence intervals indicated by the dotted line, n=3.

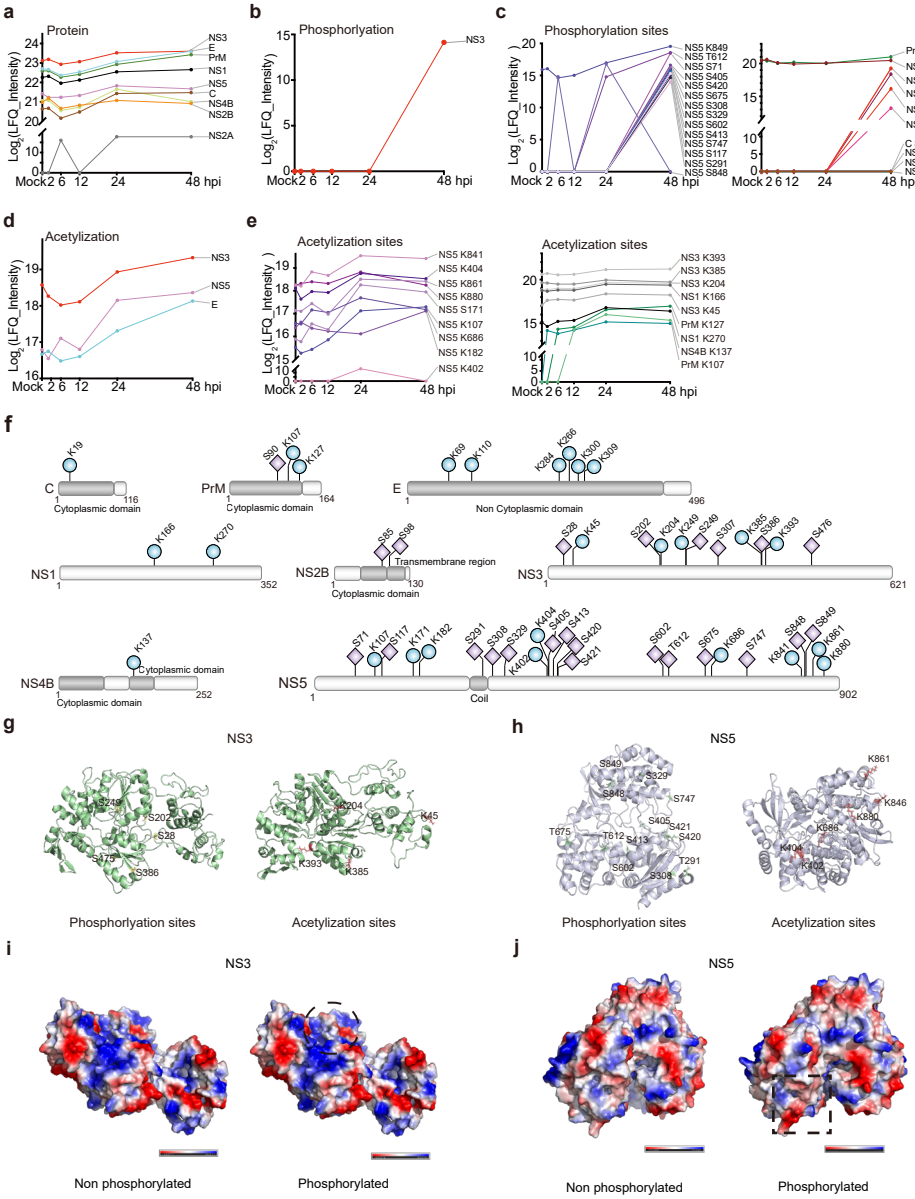

Figure S3. **Acetylation and phosphorylation modifications of viral proteins**

a. Abundance of individual TBEV viral proteins measured by proteomics analysis.

b-e. Phosphorylated NS3 protein (**b**), acetylated NS3, NS5 and E proteins (**d**), along with phosphorylated (**c**) and acetylated sites (**e**) on TBEV proteins. The number represents the specific location of phosphorylation or acetylation.

f. Phosphorylation (purple squares) and acetylation (blue circles) sites on C, prM, E, NS1, NS2A, NS2B, NS3, NS4B and NS5 at 48 hpi.

g, h. Mapping of acetylation and phosphorylation sites onto the crystal structure of NS3 (g) and NS5 (h).

i, j. Analysis of the electrostatic surface potential for both non-phosphorylated and phosphorylated TBEV NS3 (**i**) and NS5 (**j**). The red regions indicate areas with negative electrostatic potential, white corresponds to neutral regions, and blue signifies areas with positive electrostatic potential.

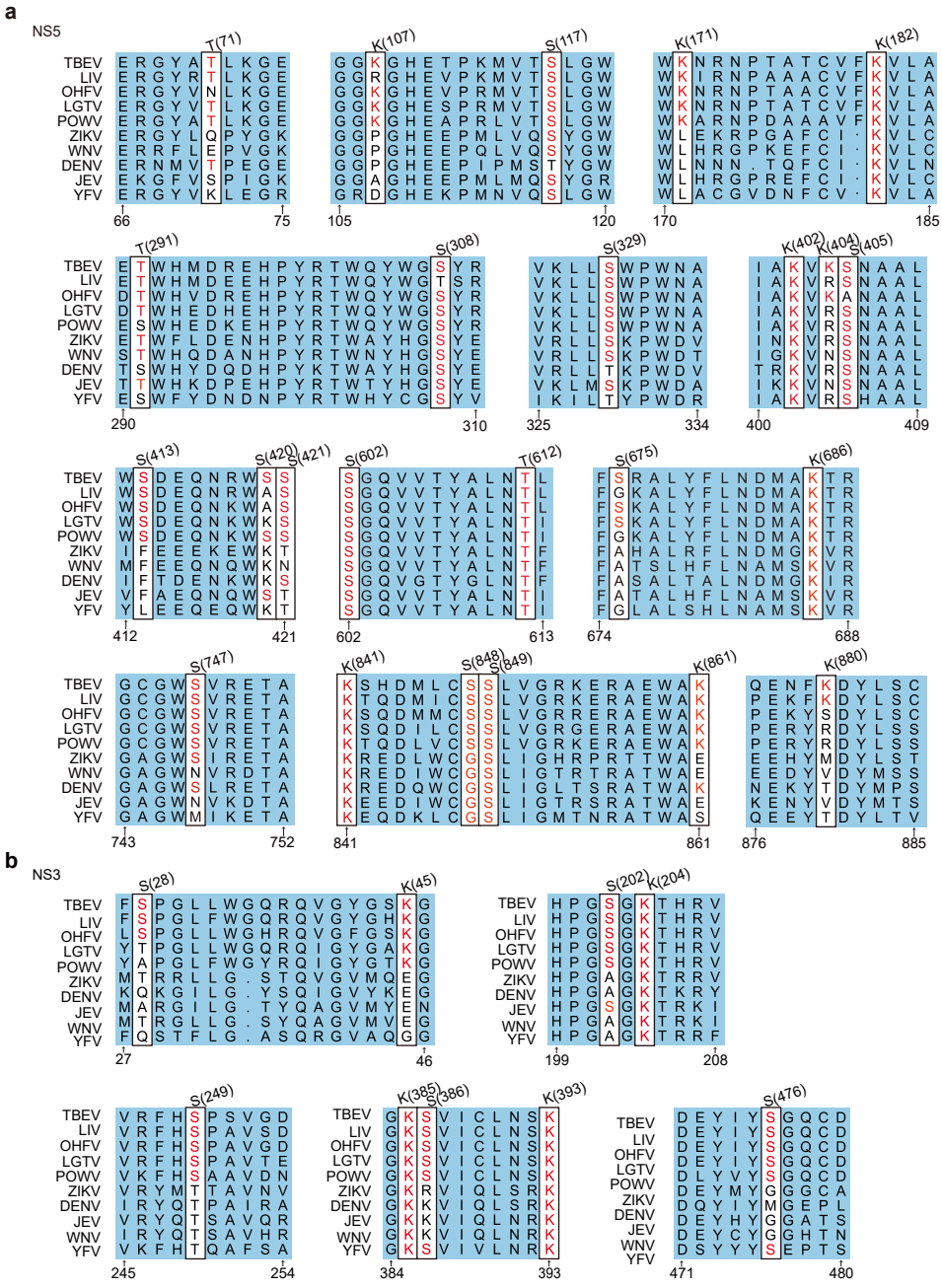

Figure S4. Conserved acetylated and phosphorylated sites on TBEV NS3 and NS5 with the other flaviviruses

a. Amino acid sequence alignment of TBEV NS5 with other flaviviruses.

b. Amino acid sequence alignment of TBEV NS3 protein with other flaviviruses.

LIV, Louping ill virus; OHFV, Omsk hemorrhagic fever virus; LGTV, Langat virus; POWV, Powassan virus; ZIKV, Zika virus; DENV, dengue virus; JEV, Japanese encephalitis virus; YFV, yellow fever virus

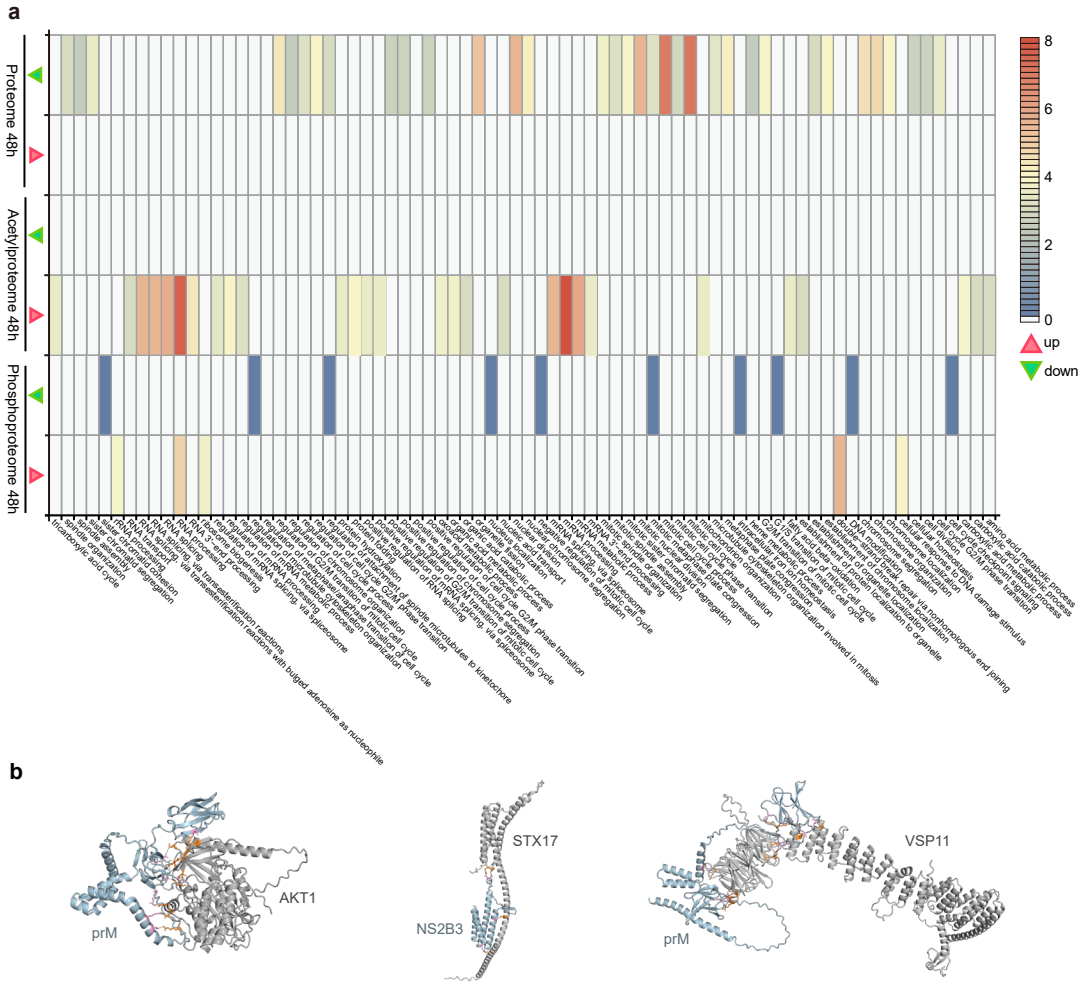

Figure S5. GO enrichment analysis of multi-proteome after TBEV infection and the interaction analysis between host and viral proteins

a. The figure displays significantly enriched GO pathways across upregulated (red arrow) or downregulated (green arrow) protein, acetylation, and phosphorylation profiles at 48 hours post TBEV infection. Enrichment was determine using Fisher's exact test with an unadjusted *P*-value $\leqslant$ 0.05.

b. Interaction analysis of prM-AKT1, NS2B3-STX17 and prM-VPS11.

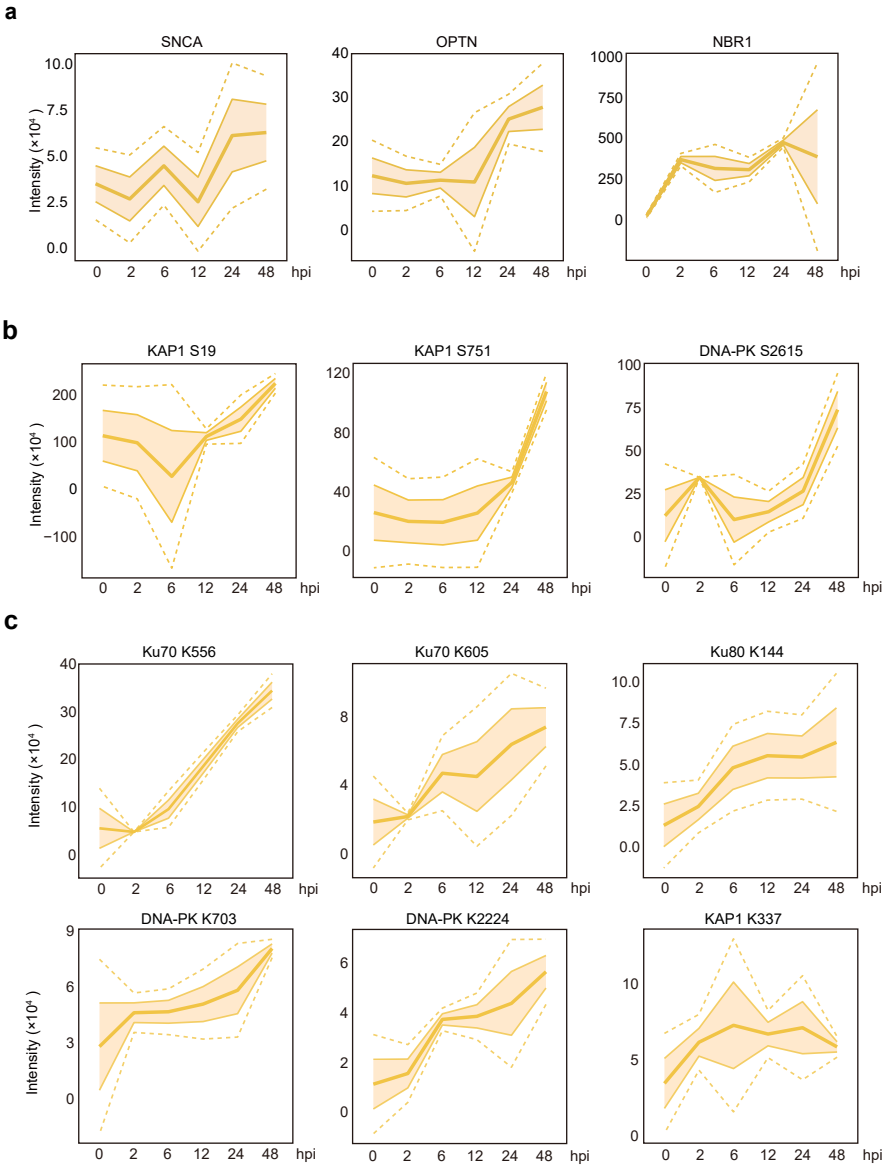

Figure S6. TBEV infection affects cellular autophagy and DNA damage response in infected cells

a. Dynamics of the abundance of SNCA, OPTN, and NBR1 modulated in TBEV-infected cells. Depicted with the median (line), 50% (shaded region) and 95% (dotted line) confidence intervals, n=3.

b. Temporal alterations in acetylation at specific sites of KAP1 (S19, S751) and DNA-PK (S2615) post-infection, as depicted by profile plots, depicted by profile plots, based on data from three independent trials.

c. Profile plots highlighting changes in phosphorylation at distinct loci on Ku70 (K334, K605), Ku80 (K144), DNA-PK (K703, K337, K2224), and KAP1 (K337) following infection, based on data from three independent trials.

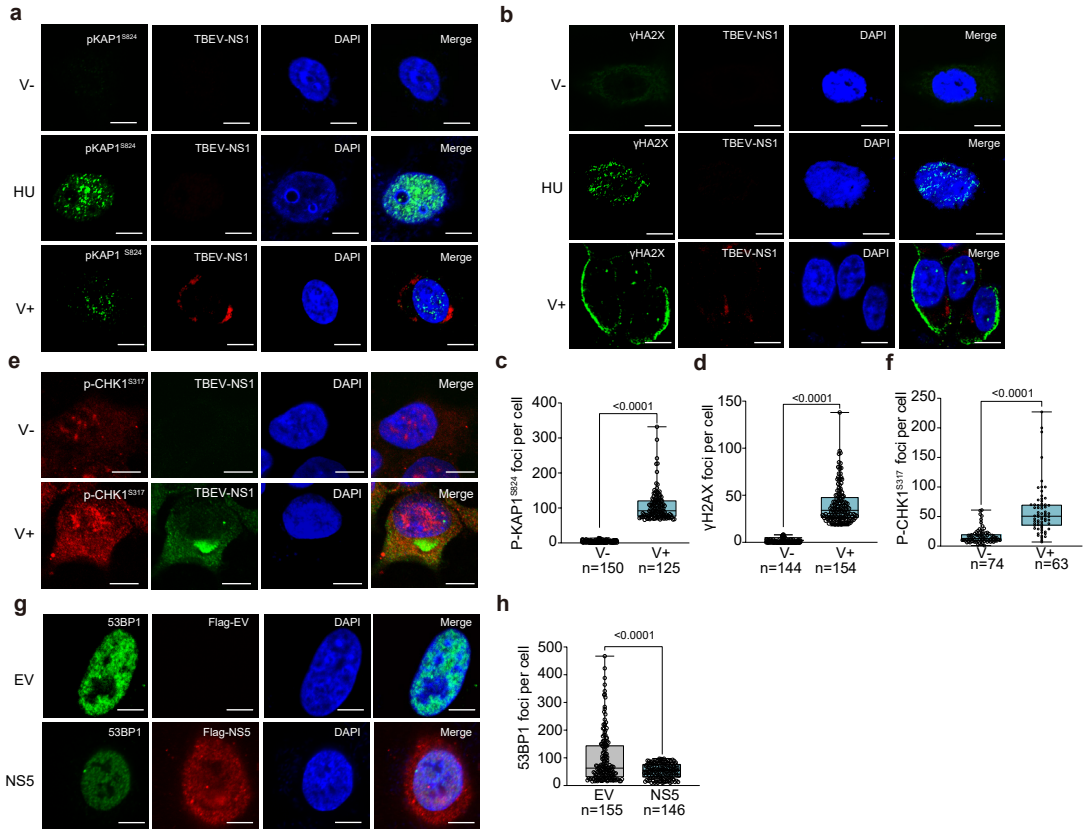

Figure S7. TBEV activates DNA damage response in infected cells

a, b, e. Cells infected with TBEV at 24 hpi displayed an increased formation of punctate structures for pKAP1^{S824} (**a**), γH2AX (**b**) and pCHK1^{S317} (**e**)compared with control cells. TBEV NS1 protein labelled infected cells. Nuclei were counterstained with DAPI. Scale bar, 10 μm.

c. Quantification of puncta in (**a**) revealed a significant difference, with each dot representing a nucleus. Data are shown as mean ± SEM (V-, n=150 cells; V+, n=125 cells).

d. Quantification of puncta in (**b**) showed a similar trend, with each data point representing a nucleus. Data are shown as mean ± SEM (V-, n=144 cells; V+, n=154 cells).

f. Quantification of puncta in (**e**) showed a similar trend, with each data point representing a nucleus. Data are shown as mean ± SEM (V-, n=74 cells; V+, n=63 cells).

g. Cells transfected with Flag-NS5 exhibited a decrease formation of punctate structures for 53BP1 compared with the empty vector transfection group. Scale bar, 5 μm.

h. Quantification of puncta in (**g**), with each dot representing a nucleus. Data are shown as mean ± SEM (V-, n=182 cells; V+, n=169 cells).

Each point represents a sample. Data are represented as mean ± SEM of 3 independent experiments. For all boxplots (c, d, f, h), median, upper and lower quartile as well as significance levels of P values from two-sided Wilcoxon test are shown. Source data are provided as a Source Data file.

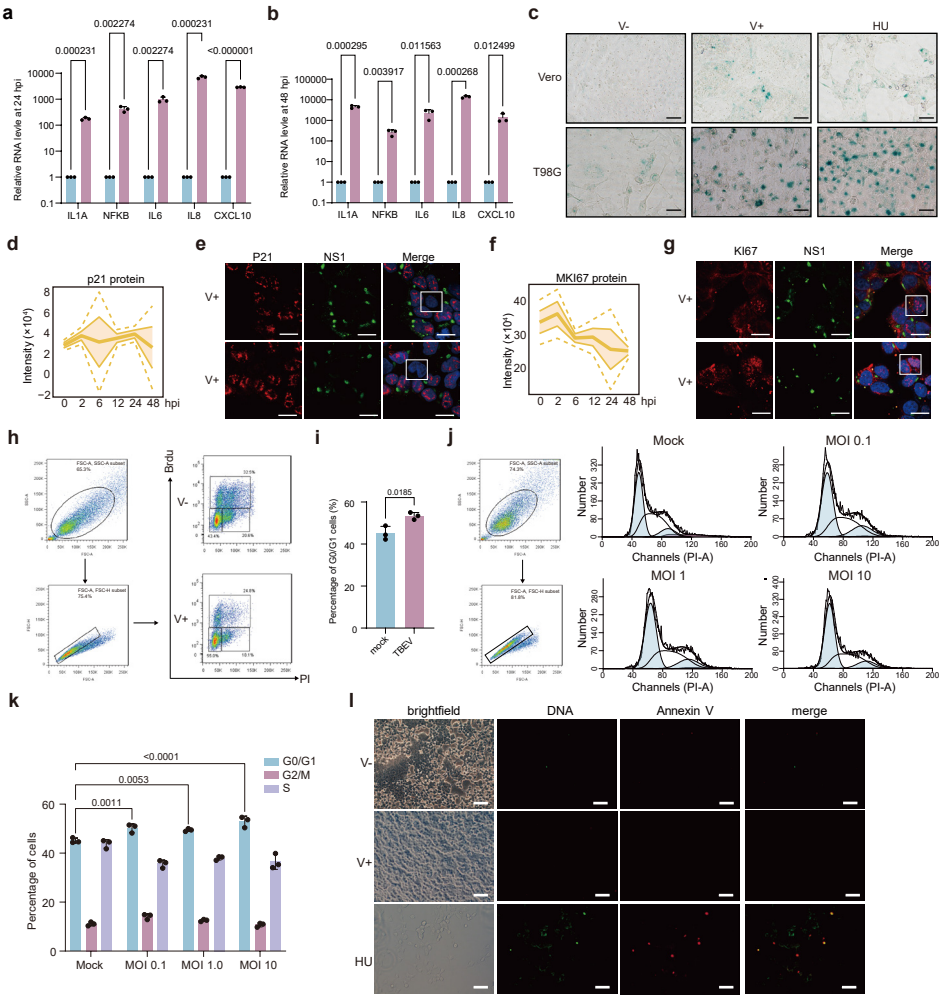

Figure S8. TBEV dysregulates cellular senescence markers and cell cycle.

a-b. qPCR assay showing increased levels of genes associated with cellular inflammatory factors (*IL1A, NFKB, IL6, IL8, CXCL10*) in TBEV-infected cells at 24 hpi (**a**) and 48 hpi (**b**)

c. Cells infected with TBEV 24 hpi showed more senescence-associated β-galactosidase staining compared with control cells. Scale bar, 100 µm.

d-g. Regulation of the protein abundance of P21 and MKI67 analyzed by proteomics (**d, f**) and IFC staining (**e, g**) in TBEV-infected cells. The graph is depicted with the median (line), 50% (shaded region) and 95% (dotted line) confidence intervals, n=3.

h. FACS analysis of TBEV-infected cells by BrdU identify higher percentage of G0/G1 cells upon TBEV infection.

i. Quantification of G0/G1 cells shown in (**h**).

j. FACS analysis of TBEV-infected cells revealed G0/G1 cell cycle arrest.

k. Percentage of cells in G0/G1, S and G2/M was quantified based on the FACS analysis in (**j**).

l. Cells infected with TBEV at 24 hpi showed no effect on Annexin-V/Caspase-3 staining associated with apoptosis compared with control cells. Scale bar, 100 µm.

Data are represented as mean ± SEM of 3 independent experiments. Each point represents a sample. The P-values are calculated and reported using one-way ANOVA. (a, b, i, k) Source data are provided as a Source Data file.

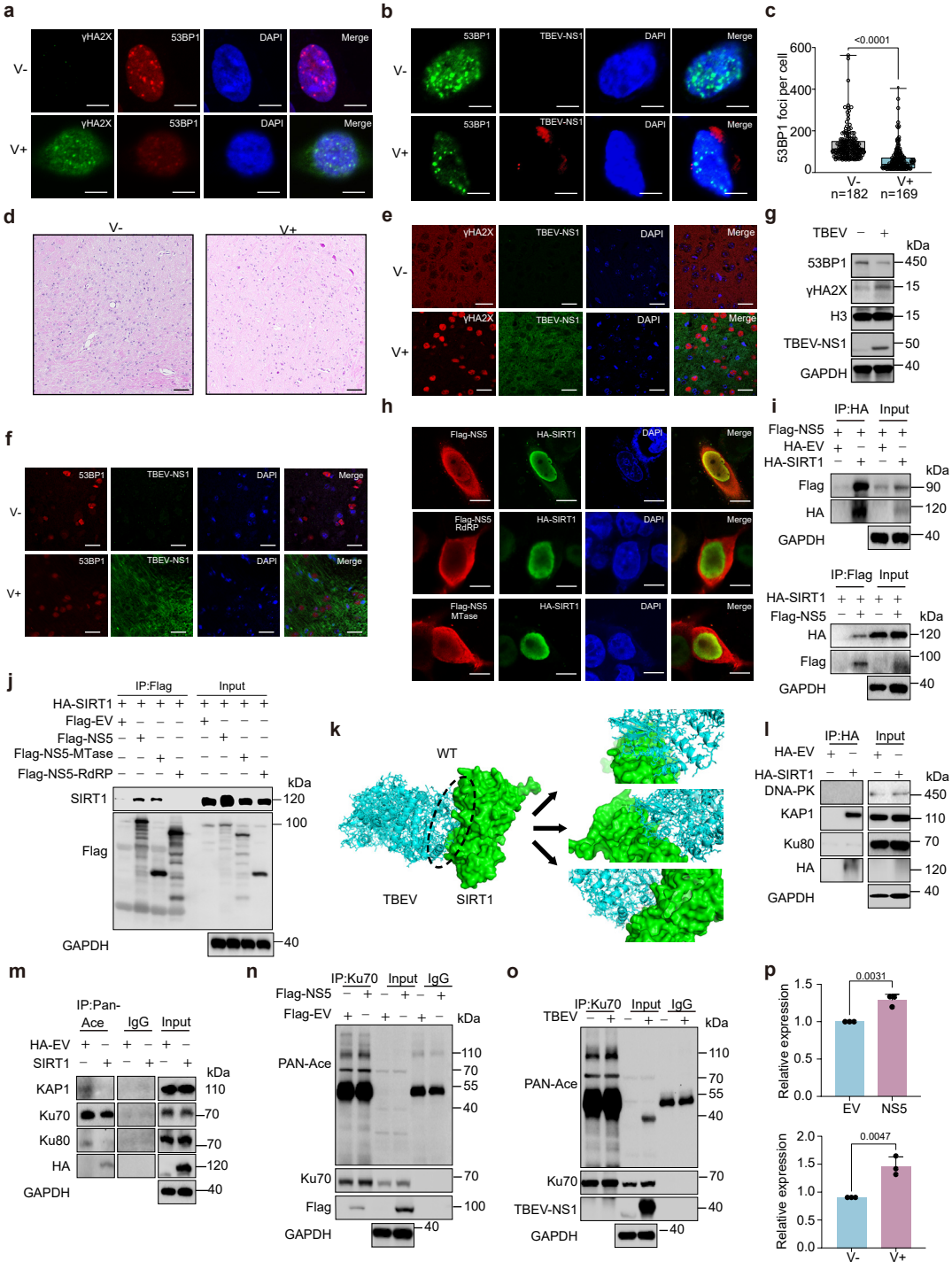

Figure S9. TBEV NS5 interferes with host DDR through interacting with SIRT1.

a. Colocalization of 53BP1 and γH2AX punctate structures in cells infected with TBEV at 24 hpi compared with control cells. Scale bar, 5 μm.

b. Cells infected with TBEV at 24 hpi exhibited a decrease formation of punctate structures for 53BP1 compared with control cells. Scale bar, 5 μm.

c. Quantification of puncta in (**b**), with each dot representing a nucleus. Data are shown as mean ± SEM (V-, n=182 cells; V+, n=169 cells).

d. H&E staining of mock and TBEV-infected brain of mice. Scale bar, 50 μm.
e-f. Brain organoids infected with TBEV displayed an increased formation of punctate structures for γH2AX(**e**) but decreased 53BP1 (**f**) compared with control brain organoids. Scale bar, 20 μm.
g. Immunoblot assays demonstrated a significant decrease in the levels of 53BP1 but an increased γH2AX protein in mice tissue infected with TBEV compared to control mice.
h. Flag-NS5 co-localized with HA-tagged SIRT1, visualized by anti-HA (green) and anti-Flag (red) antibodies. Scale bars, 10 μm.
i. Co-precipitation of endogenous (*up*) and overexpressed SIRT1(*down*) by Flag-NS5 in coimmunoprecipitation assay.
j. Co-precipitation of overexpressed SIRT1 by Flag-NS5 and its truncated fragments in coimmunoprecipitation assay.
k. Interaction analysis indicated that 8 amino acids on TBEV NS5 (ARG^{34}, GLU^{28}, GLU^{24}, GLU^{175}, ARG^{184}, GLU^{17}, ASP^{14}, LEU^{22}) involved in its interaction with SIRT1.
i. Endogenous KAP1 co-precipitated by HA-SIRT1 in coimmunoprecipitation assay, while no obvious interaction observed between SIRT1 with DNA-PK or Ku80.
m. Co-immunoprecipitation assay demonstrated reduced acetylation of KAP1, Ku70 and Ku80 in SIRT1- overexpressed cells.
n-p. Levels of acetylated Ku70, precipitated by anti-ku70 antibody, were elevated in NS5 overexpressed (**n**) and TBEV-infected (**o**) cells compared to the control cells. Quantification of acetylated KAP1, Ku70 and Ku80 in NS5 overexpressed and TBEV-infected (p) cells.
Data are represented as mean ± SEM of 3 independent experiments. Each point represents a sample. The P-values are calculated and reported using one-way ANOVA. For all boxplots (c), median, upper and lower quartile as well as significance levels of P values from two-sided Wilcoxon test are shown. Source data are provided as a Source Data file.

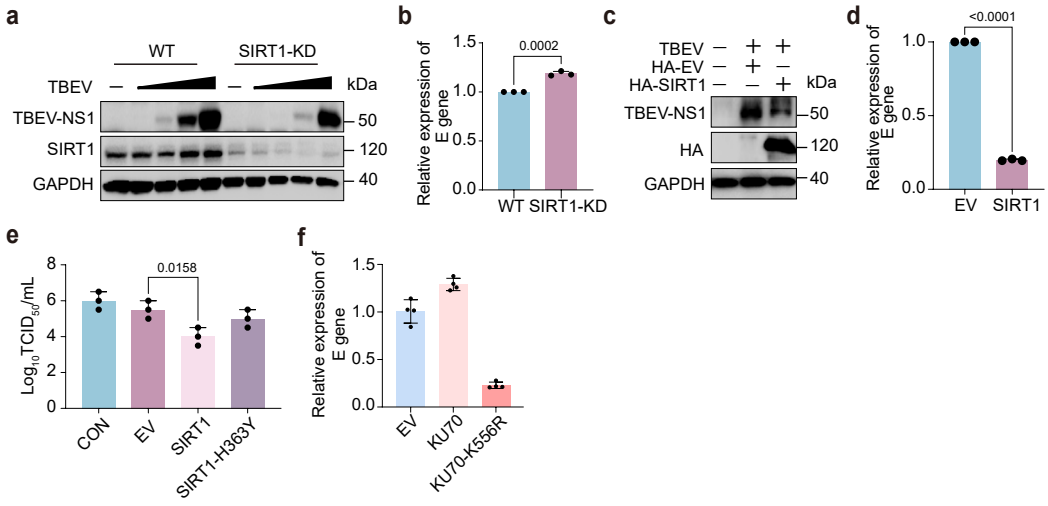

Figure S10. The inhibitory effect of SIRT1 on TBEV replication

a. TBEV-NS1 protein exhibited no significantly change in HEK293T cells or HEK293T-SIRT1-KD (knockdown) cells analyzed by immunoblot assays.

b. Knockdown of SIRT1 led to a slight elevation in the mRNA level of TBEV E gene, as quantified by probe PCR.

c. Immunoblot assays demonstrated a significant decrease in the levels of TBEV NS1 protein in cell overexpressing HA-SIRT1 compared to cell transfected with an empty vector (EV).

d. Probe PCR analysis indicated a reduction in the mRNA level of TBEV E genes in SIRT1 overexpressed cells compared with empty vector transfected cells**.**

e. $TCID_{50}$ assay showed a decrease in the titer of TBEV in cells overexpressing SIRT1, but not in cells transfected with SIRT1-H363Y.

f. Probe PCR analysis indicated a reduction in the mRNA level of TBEV E genes in ku70-K556R overexpressed cells compared with empty vector transfected cells.

Data are represented as mean ± SEM of 3 independent experiments. Each point represents a sample. The P-values are calculated and reported using one-way ANOVA. (b, d, e, f). Source data are provided as a Source Data file.

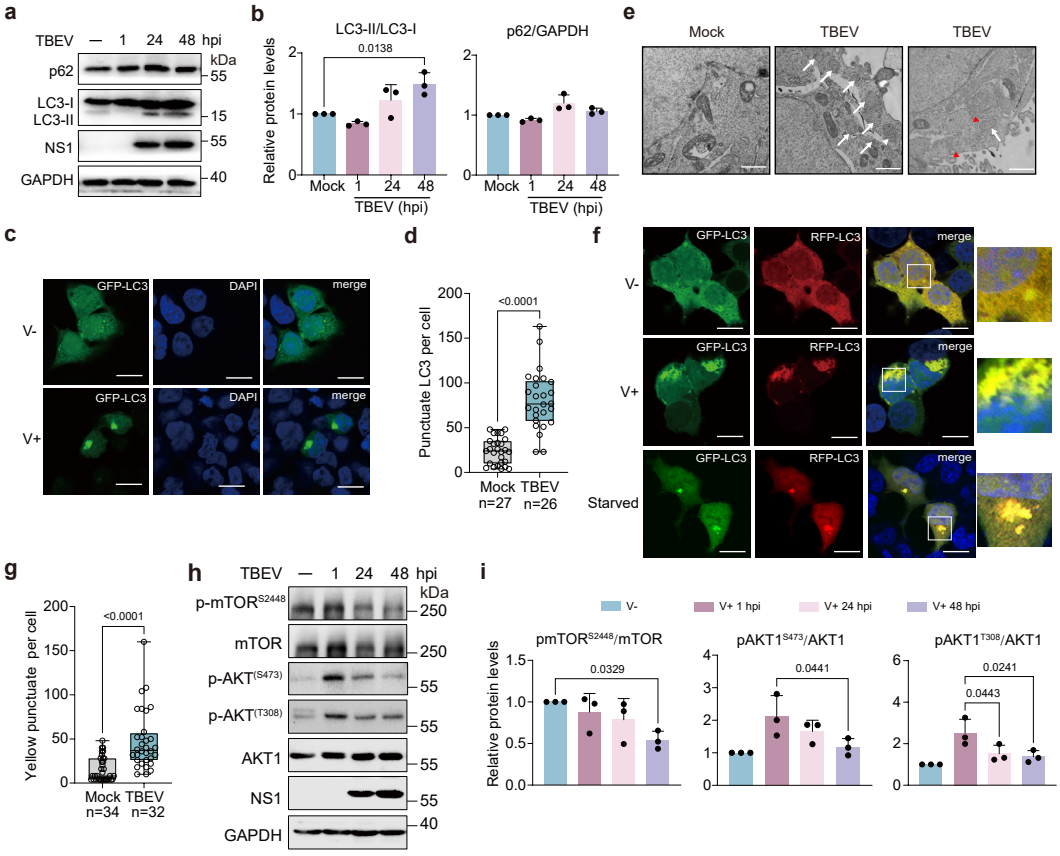

Figure S11. TBEV infection induces autophagy while concurrently blocks autophagic flux.
a. Immunoblot assay revealed an increase in the relative expression level of LC3-II/LC3-I and no significant change of P62 in TBEV-infected cells.
b. Quantification demonstrated an elevated percentage of LC3-II/LC3-I and p62/GAPDH in TBEV-infected cells.
c. TBEV-infected cells exhibited a higher number of GFP^{+}LC3 puncta compared with mock-infected cells. Scale bar, 20 μm.
d. Quantification of the number of GFP^{+} LC3 puncta per cell confirmed the increase in autophagosomes in TBEV-infected cells. (mock, n=27 cells; TBEV, n=26 cells)
e. TEM analysis indicated a higher accumulation of autophagosomes (white arrows) accumulated in TBEV-infected cells compared to mock-infected cells. The red arrowheads indicate virion particles, the white arrows indicate double-membrane autophagosomes. Scale bar, 1 μm.
f. Cells infected with TBEV displayed more yellow $GFP^{+}RFP+$LC3 puncta compared to mock-infected cells. Scale bar, 20 μm.
g. Quantification of the number of $GFP^{+}RFP^{+}$ LC3 puncta per cell confirmed impairment of autophagic flux in TBEV-infected cells. (mock, n=34 cells; TBEV, n=32 cells)
h. Immunoblot assay showed a decrease in the phosphorylated forms of AKT1 (S473 and T308) and mTOR (S2448) in cells infected with TBEV at 24 and 48 hpi.
i. Quantification confirmed the decreased levels of phosphorylated proteins in (**h**).
Data are represented as mean ± SEM of 3 independent experiments. Each point represents a sample. The P-values are calculated and reported using one-way ANOVA. (b, i). For all boxplots (d, g), median, upper and lower quartile as well as significance levels of P values from two-sided Wilcoxon test are shown. Source data are provided as a Source Data file.

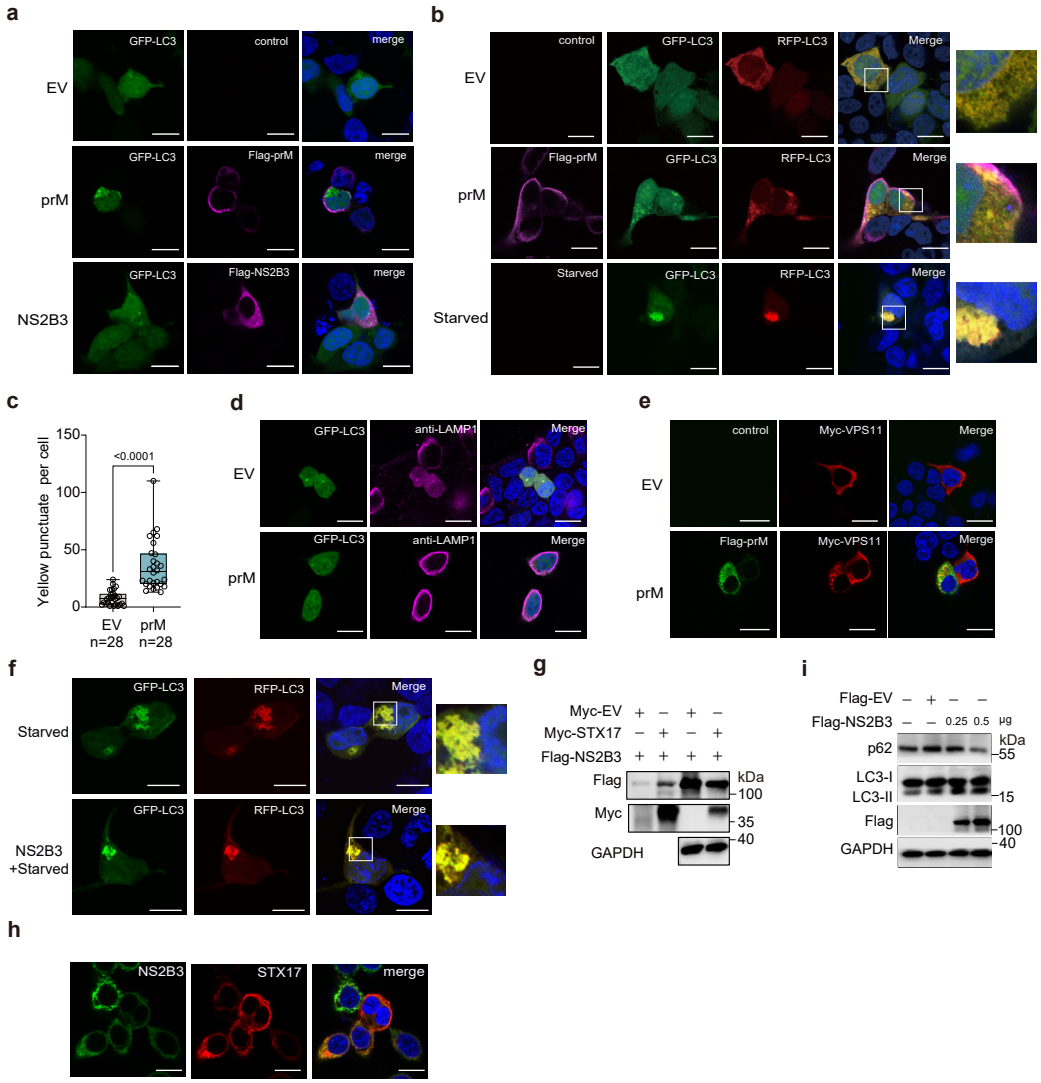

Figure S12. The impact of prM on autophagy induction and autophagic flux inhibition.
a. Cells overexpressing prM displayed an increased number of $GFP^{+}LC3$ puncta compared to cells overexpressing EV and NS2B3. Scale bar, 10 μm.
b. Cells expressing prM exhibited a higher number of $GFP^{+}RFP^{+}$ LC3 puncta compared to control cells. Scale bar, 10 μm.
c. Quantification of the number of $GFP^{+}RFP^{+}$ LC3 yellow puncta per cell in (**b**). (EV, n=28 cells; prM, n=28 cells)
d. In prM-expressing cells, LC3 puncta were notably distinct from lysosomes labeled LAMP1. Scale bar, 20 μm.
e. VPS11, which was largely diffuse in control cells, formed punctate structures that co-localized with prM. Scale bar, 10 μm.
f. Cells expressing NS2B3 exhibited a higher number of $GFP^{-}RFP^{+}$ LC3 puncta compared to control cells. Scale bar, 10 μm.
g. Co-immunoprecipitation demonstrating the interaction between overexpressed NS2B3 and STX17.
h. Colocalization of TBEV-NS2B3 with STX17 in the cytoplasmic. Scale bar, 10 μm.
i. Immunoblot assay revealed an increase in the expression level of LC3-II while decreased level of P62 in TBEV-infected cells.
Data are represented as mean ± SEM of 3 independent experiments. For all boxplots (c), median, upper and lower quartile as well as significance levels of P values from two-sided Wilcoxon test are shown. Source data are provided as a Source Data file.

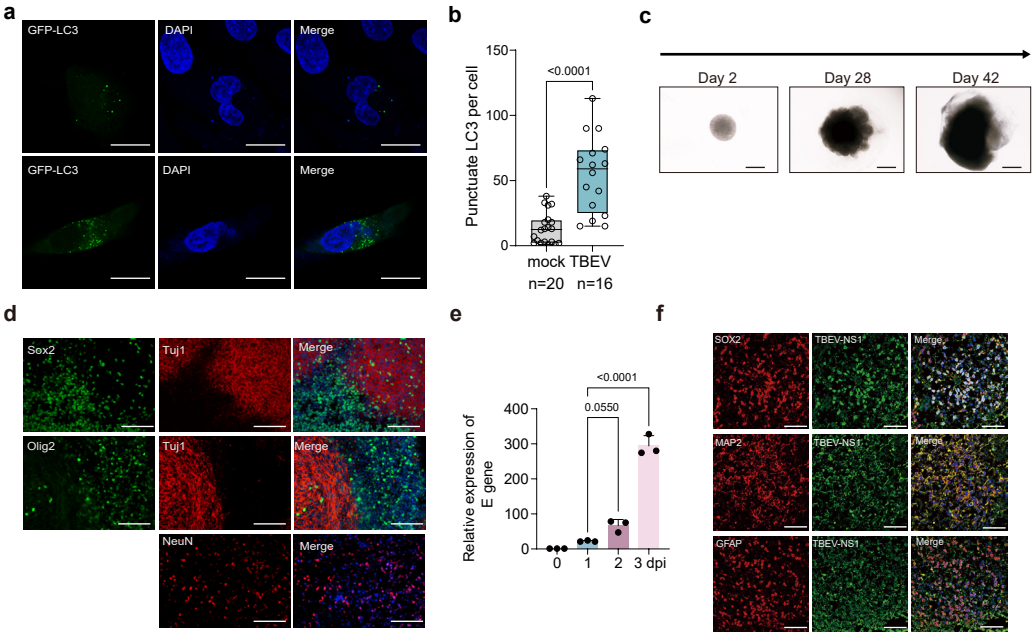

Figure S13. TBEV infection regulates DNA damage response and autophagy in T98G cells and brain organoids

a. TBEV-infected cells exhibited a higher number of GFP^{+}LC3 puncta compared with mock-infected cells. Scale bar, 20 µm.

b. Quantification of the number of GFP^{+} LC3 puncta per cell confirmed the increase in autophagosomes in TBEV-infected cells. (V-, n=20 cells; V+, n=16 cells)

c. An overview of the generation of brain organoids from iPSC. Scale bar, 500 µm.

d. Images showcased 42-day-old organoids from iPSC, highlighting markers TUJ1 (neurons), SOX2 (progenitors), Olig2 (oligodendrocyte), and NeuN (nucleus of neurons). White arrows indicated rosette-like structures. Scale bar, 100 µm.

e. Quantification by probe PCR demonstrated a gradual increase in the copies of TBEV E genes with the duration of TBEV infection

f. Immunofluorescence analysis highlighted the colocalization of TBEV NS1 with SOX2 (progenitors), MAP2 (neurons), GFAP (astroglia). Scale bar, 200 µm.

Data are represented as mean ± SEM of 3 independent experiments. Each point represents a sample. The P-values are calculated and reported using one-way ANOVA. (e). For all boxplots (b), median, upper and lower quartile as well as significance levels of P values from two-sided Wilcoxon test are shown. Source data are provided as a Source Data file.

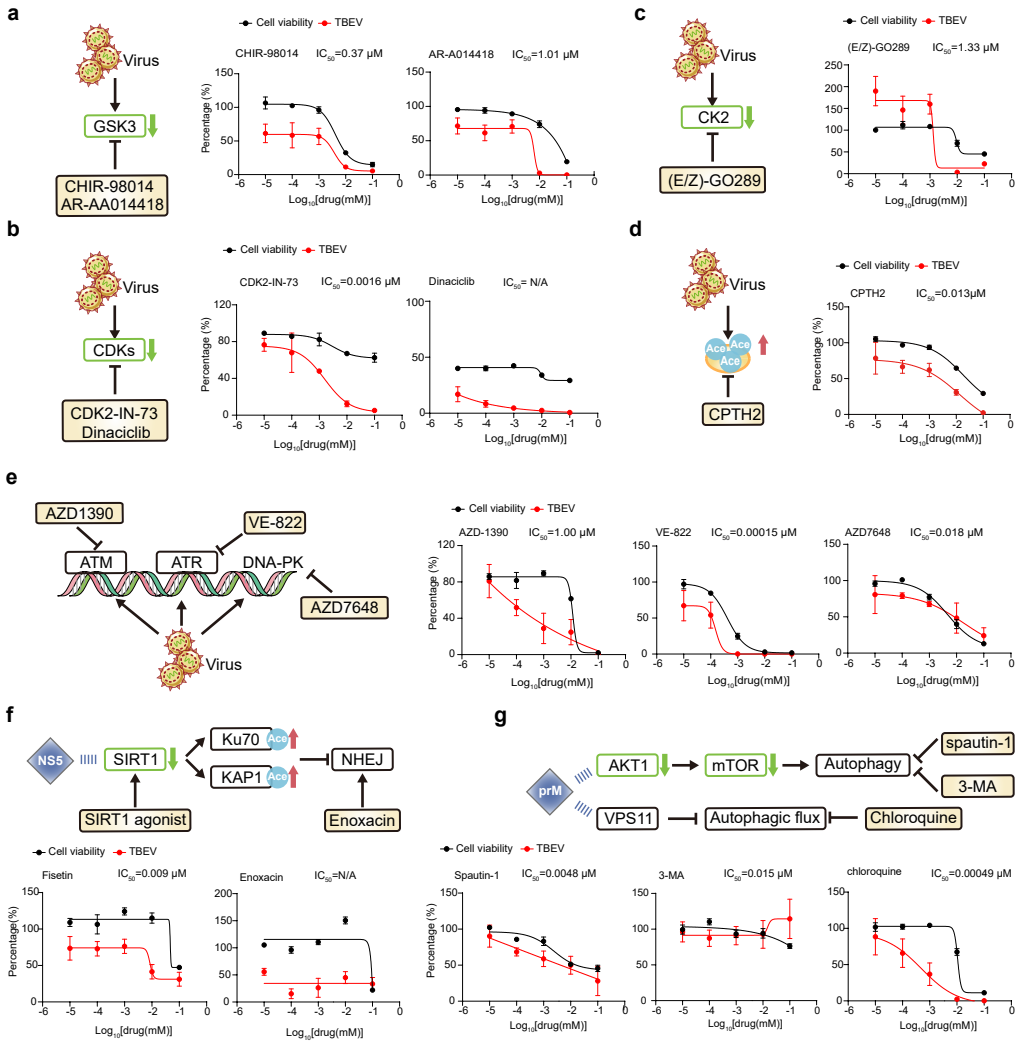

Figure S14. Pharmacological modulation of host factors reduces TBEV replication in A549 cells

a. TBEV infection inhibits the activity of GSK3. Vero cells were pre-treated with inhibitors of GSK3, CHIR-98014 and AR-A014418 at the indicated doses, followed by TBEV infection for 48 h, IC_{50} values were detected by probe PCR. The cell viability was measured by cell counting (CCK-8) assay without viral infection. Percent of viral titer compared with DMSO treatment (red) and cell viability (black) is depicted. Error bars represent the mean ± SEM of three biological replicates.

b, c. Similar to (**a**), A549 cells were treated with the CDK2 inhibitor CDK2-IN-73, Dinaciclib (**b**) and CK2 inhibitor (E/Z)-GO289 (**c**).

d. TBEV infection elevates the acetylation of host proteins. A549 cells were pre-treated with the acetylase inhibitor (CPTH2) before TBEV infection.

e. TBEV infection activates ATM, ATR, and DNA-PK to induce DNA damage response. A549 cells were pre-treated with the inhibitors of ATM (AZD1390), ATR (VE-822) and DNA-PK (AZD7648) prior to TBEV infection.

f. TBEV NS5 binds to SIRT1 and inhibits its activity to repress DNA damage repair. A549 cells were pre-treated with the SIRT1 agonist (Fisetin) and a DNA damage repairment (Enoacxin) before TBEV infection.

g. TBEV prM interacts with AKT1 and VPS11 to regulate autophagy. A549 cells were pre-treated with autophagy inhibitors (Spautin-1 and 3-MA) and autophagic flux (chloroquine) prior to TBEV infection. Error bars represent the mean ± SEM of three biological replicates. Source data are provided as a Source Data file.

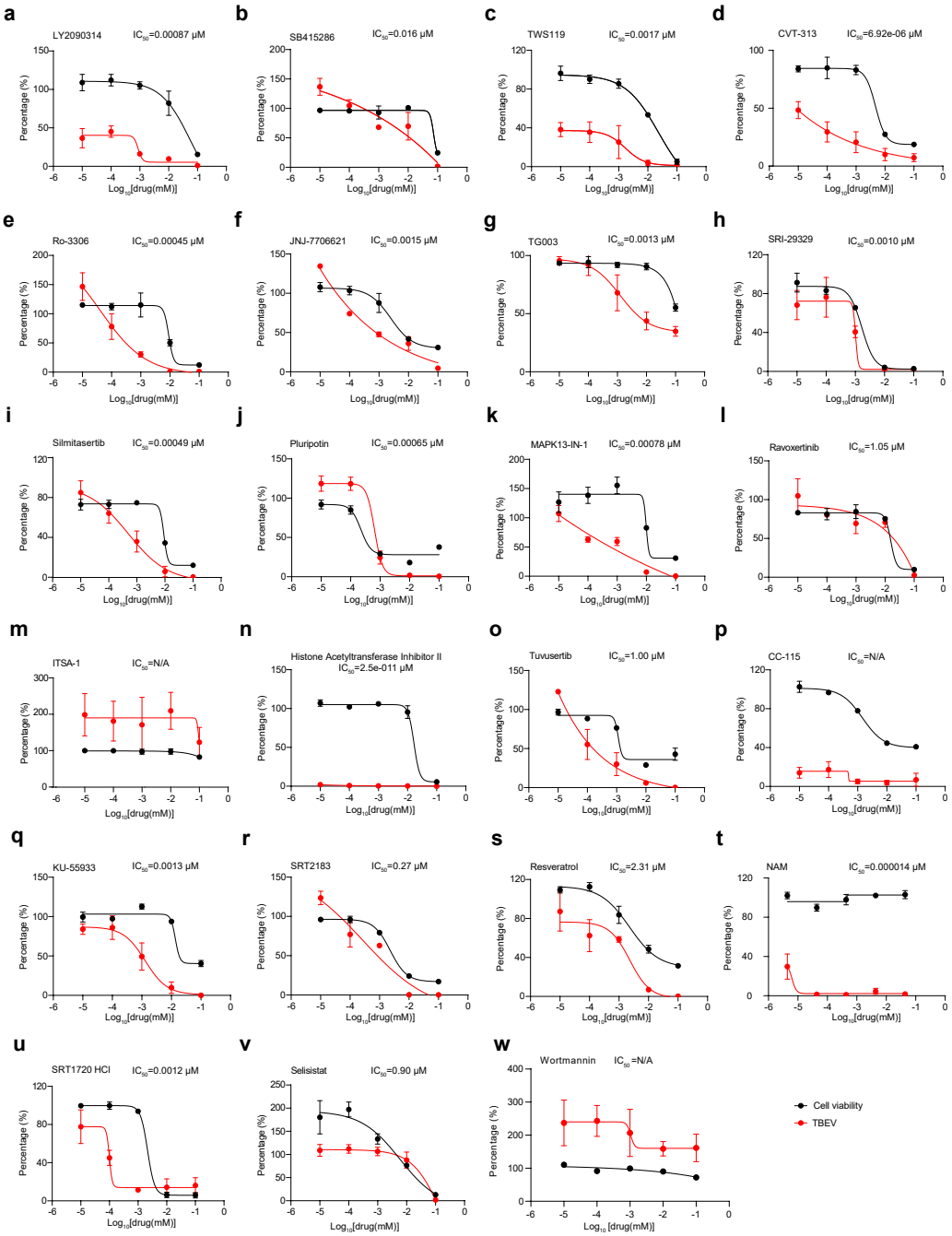

Figure S15. Pharmacological profiling for viral titers and cell viability in Vero cells.
Cells were pretreated with the indicated drugs and then infected with TBEV for 48 h. IC_{50} values were detected by probe PCR. The cell viability was measured by cell counting (CCK-8) assay without viral infection. The red line indicates the effects in infection measured at each drug dose. The black line shows cell viability at each drug dose. Each drug was tested in three independent repeated experiments, and error bars represent the mean ± SEM of three biological replicates. Source data are provided as a Source Data file.

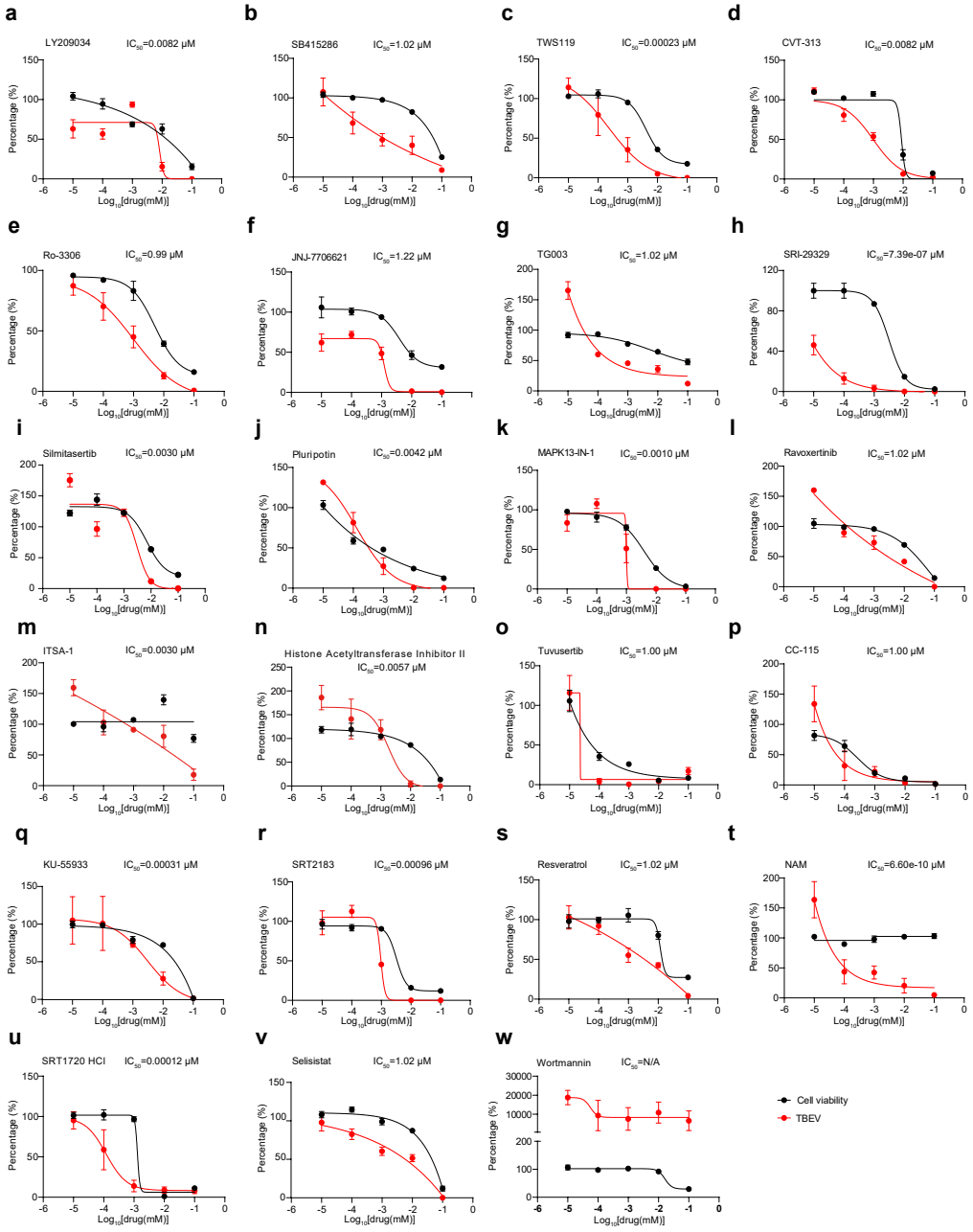

Figure S16. Pharmacological Profiling for viral titers and cell viability in A549 cells.
Cells were pretreated with the indicated drugs and then infected with TBEV for 48 h. IC_{50} values were detected by RT-PCR. The cell viability was measured by a cell counting (CCK-8) assay without viral infection. The red line indicates the effects in infection measured at each drug dose. The black line shows cell viability at each drug dose. Each drug was tested in three independent repeated experiments, and error bars represent the mean ± SEM of three biological replicates. Source data are provided as a Source Data file.

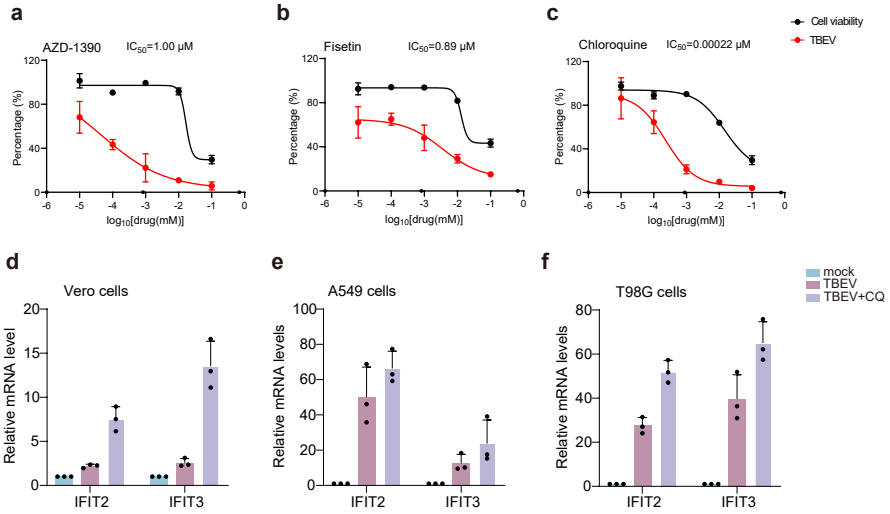

Figure S17. Pharmacological Profiling for viral titers and cell viability in T98G cells.
a-c. ATM inhibitor (AZD-1390), SIRT1 agonist (Fisetin), and autophagic flux inhibitor (chloroquine) significantly inhibited the transcription of TBEV E genes in T98G cells.
d-e. Vero (**d**), A549 (**e**) and T98G cells (**f**) were either mock-infected or infected with TBEV, along with some cells were pre-treated with 1 μM chloroquine (CQ) prior to TBEV infection. Following these treatments, the cells were harvested, and the mRNA expression levels of IFIT2 and IFIT3 were assessed.
Data are represented as mean ± SEM of 3 independent experiments. Each point represents a sample. The P-values are calculated and reported using one-way ANOVA (d-e). Source data are provided as a Source Data file.